Eur. Phys. J. C 17, 399–405 (2000)
Digital Object Identifier (DOI) 10.1007/s100520000476

THE EUROPEAN PHYSICAL JOURNAL C

On measurement of helicity parameters in top quark decay

C.A. Nelson[a], L.J. Adler, Jr.

Department of Physics, State University of New York at Binghamton, Binghamton, NY 13902-6016, USA

Received: 10 July 2000 / Published online: 8 September 2000 – © Springer-Verlag 2000

Abstract. To enable an evaluation of future measurements of the helicity parameters for $t \to W^+b$ decay in regard to $\tilde{T}_{FS}$ violation, this paper considers the effects of an additional pure-imaginary coupling, $ig_i/2\Lambda_i$ or ig_i, associated with a specific, single additional Lorentz structure, $i = S, P, S \pm P, \ldots$. Sizable $\tilde{T}_{FS}$ violation signatures can occur for low-effective mass scales ($< 320GeV$), but in most cases can be more simply excluded by 10% precision measurement of the probabilities $P(W_L)$ and $P(b_L)$. Signatures for excluding the presence of $\tilde{T}_{FS}$ violation associated with the two dynamical phase-type ambiguities are investigated.

1 Introduction

In $t \to W^+b$ decay, it is important to be able to evaluate future measurements of competing observables consistent with the standard model (SM) prediction of only a g_{V-A} coupling and of only its associated discrete-symmetry violations. For this purpose, without consideration of possible explicit $\tilde{T}_{FS}$ violation, in [1] plots were given of the values of the helicity parameters in terms of a "$(V-A)$ + Single Additional Lorentz Structure" versus effective-mass scales for new physics, Λ_i, associated with each additional Lorentz structure. In this paper, the effects of possible explicit $\tilde{T}_{FS}$ violation are reported. In the present formulation, by "explicit $\tilde{T}_{FS}$ violation", c.f. Sect. 2, we mean an additional complex-coupling, $g_i/2\Lambda_i$ or g_i, associated with a specific single additional Lorentz structure, $i = S, P, S \pm P, \ldots$.

The main motivation for the present analysis are the observed CP and T violations in K^0 decay. Although these discrete-symmetry violations are empirically well-described by the CKM matrix which describes the linear superposition of the quark mass eigenstates which appears in the phenomenological weak eigenstates, the fundamental origin of these symmetry violations is still unknown. Experimental results should soon be available about whether the CKM formulation is also successful in b-quark decay. In the case of the strong interactions, there is the opposite difficulty of a fundamental strong CP problem which has led to the prediction of the existence of axions, the Nambu-Goldstone bosons associated with a global $U(1)_{PQ}$ symmetry. These axions have yet to be discovered. Lastly, and perhaps more significantly for t-quark decay, most astrophysics studies of electroweak baryogenesis conclude that additional sources of CP violation, beyond CKM, in elementary particle physics are necessary to explain the observed baryon-to-photon ratio. So in spite of the robustness of the standard model and of the CKM formulation, perhaps after all, t-quark decay is not the wrong place to look for CP and T violations.

A first measurement of the longitudinal W boson fraction was reported in [2]. A recent working group review of t-quark physics is in [3]. A recent review of CP violation in t-quark physics is in [4]. Besides these references and those listed in [1], some of the related recent literature is [5-14].

The present analysis assumes that future measurements of $t \to W^+b$ decay will be at least approximately consistent with the SM prediction of only a g_{V-A} coupling. If the SM is correct, one expects that the $A(0,-1/2)$ and $A(-1,-1/2)$ moduli and relative phase β_L will be the first quantities to be somewhat precisely determined. As shown by Table 1, the $\lambda_b = 1/2$ moduli are factors of 30 and 100 smaller in the SM. The helicity parameters appear directly in various polarization and spin-correlation functions for $t \to W^+b$ decay such as those obtained in [15]. By measurement of independent helicity parameters, or from other empirical analyses of spin-correlation and polarization observables, it will be possible to test in several independent ways that the R-handed b-quark amplitudes, $\lambda_b = 1/2$, are indeed negligible to good precision. Eventually there should also be direct evidence for their existence if the SM is correct.

If the R-handed amplitudes are negligible, then besides $P(b_L) \simeq 1$ it follows that $\zeta \simeq 2P(W_L) - P(b_L)$ and that $\omega \simeq \eta$. Showing an approximate empirical absence of R-handed amplitudes would also be useful in regard to tests for $\tilde{T}_{FS}$ violation: Assuming that the L-handed amplitudes dominate, the $\eta_L^{'}$ helicity parameter satisfies the relation $(\ \eta_L^{'})^2 \cong \frac{1}{4}[P(b_L)+\zeta][P(b_L)-\zeta] - (\ \eta_L)^2$. For instance, in the SM the vanishing of the right-hand-side is due to the vanishing of $\sin\beta_L$ provided that the R-handed amplitudes are negligible. If $\tilde{T}_{FS}$ violation were to occur, besides normally a non-zero approximate-equality in the

[a] e-mail: cnelson @ binghamton.edu

Table 1. For the standard model and at the ambiguous moduli points, numerical values of the associated helicity amplitudes $A(\lambda_{W^+}, \lambda_b)$. The values for the amplitudes are listed first in $g_L = 1$ units, and second as $A_{new} = A_{g_L=1}/\sqrt{\Gamma}$ which removes the effect of the differing partial width, Γ for $t \to W^+b$. [$m_t = 175GeV$, $m_W = 80.35GeV$, $m_b = 4.5GeV$]

	$A(0,-\frac{1}{2})$	$A(-1,-\frac{1}{2})$	$A(0,\frac{1}{2})$	$A(1,\frac{1}{2})$
$A_{g_L=1}$ in $g_L = 1$ units				
$V-A$	338	220	−2.33	−7.16
$S+P$	−338	220	−24.4	−7.16
f_M+f_E	220	−143	1.52	−4.67
$A_{New} = A_{g_L=1}/\sqrt{\Gamma}$				
$V-A$	0.84	0.54	−0.0058	−0.018
$S+P$	−0.84	0.54	−0.060	−0.018
f_M+f_E	0.84	−0.54	0.0058	−0.018

above relation, there would normally also be a non-zero $\omega' \simeq \eta'$ if the R-handed amplitudes are negligible.

Remarks on the dynamical phase-type ambiguities: Due the dominance of the L-handed amplitudes in the SM, the occurrence of the two dynamical ambiguities [1] displayed in lower part of Table 1 is not surprising because these three chiral combinations only contribute to the L-handed b-quark amplitudes in the $m_b \to 0$ limit. Since pairwise the couplings are tensorially independent, the $g_{V-A} + g_{S+P}$ and $g_{V-A} + g_{f_M+f_E}$ mixtures can each be tuned by adjusting a purely real Λ_i to reproduce, with opposite sign, the SM ratio of the two $(\lambda_W = 0, -1)$ L-handed amplitudes. Likewise, if experimental data were to suggest that the R-handed amplitudes are larger than expected, e.g. $P(b_L) \neq 1$, this might be due to the presence of additional $V+A, S-P, f_M-f_E$ type couplings. Since the $S \pm P$ couplings only contribute to the longitudinal helicity W amplitudes, they might be of interest in the case of an unexpected W longitudinal/transverse polarization ratio. Versus the upper part of Table 1, given the small m_b mass, this is the reason that the sign of the $A(0,-1/2)$ amplitude can be switched, without other important changes, by the addition of the $S+P$ coupling.

However, in the case of the $f_M + f_E$ phase-type ambiguity, from Table 1 there are 3 numerical puzzles at the mil level versus the SM values. In the upper part, the $A_+(0,-1/2)$ amplitude for $g_L + g_{f_M+f_E}$ has about the same value in $g_L = 1$ units, as the $A_{SM}(-1,-1/2)$ amplitude in the SM. As $m_b \to 0$, $\frac{A_+(-1,-1/2)}{A_{SM}(0,-1/2)} \to \frac{m_t(m_t^2-m_W^2)}{\sqrt{2}m_W(m_t^2+m_W^2)}$ $= 1.0038$. The other numerical puzzle(s) is the occurrence in the lower part of the Table 1 of the same magnitude of the two R-handed b-quark amplitudes $A_{New} = A_{g_L=1}/\sqrt{\Gamma}$ for the SM and for the case of $g_L + g_{f_M+f_E}$. Except for the differing partial width, by tuning the magnitude of L-handed amplitude ratio to that of the SM, the R-handed amplitude's moduli also become about those of the SM. With $\Lambda_{f_M+f_E}$ determined as in Sect. 3, for the A_{New} amplitudes $|A_+| - |A_{SM}| \sim (m_b/m_t)^2 = 0.0007$ versus for instance $|A_{SM}(\lambda_W, 1/2)| \propto m_b$. Of course, the row with SM values is from a "theory" whereas the row of $g_L + g_{f_M+f_E}$ values is not. Nevertheless, dynamical SSB and compositeness/condensate considerations do continue to stimulate interest [15] in additional tensorial $f_M + f_E$ couplings. In Table 1, due to the additional $f_M + f_E$ coupling, the net result is that it is the $\mu = \lambda_{W^+} - \lambda_b = -1/2$ helicity amplitudes A_{New} which get an overall sign change.

Fortunately, a sufficiently precise measurement of the sign of $|\eta_L| = 0.46$(SM) due to the large interference between the W longitudinal/transverse amplitudes can resolve the $V-A$ and f_M+f_E lines of this table. Similarly, sufficiently precise measurements of both η_L and $\eta_L{}'$ could resolve the analogous dynamical ambiguity in the case of a partially-hidden $\tilde{T}_{FS}$ violation associated with the additional $f_M + f_E$ coupling, see Fig. 7 in Sect. 3. A precise measurement of the partial width Γ could also be useful.

2 Consequences of explicit $\tilde{T}_{FS}$ violation

For $t \to W^+b$, the most general Lorentz coupling is $W_\mu^* J_{\bar{b}t}^\mu = W_\mu^* \bar{u}_b(p)\, \Gamma^\mu u_t(k)$ where $k_t = q_W + p_b$, and

$$\Gamma_V^\mu = g_V\gamma^\mu + \frac{f_M}{2\Lambda}\iota\sigma^{\mu\nu}(k-p)_\nu + \frac{g_{S^-}}{2\Lambda}(k-p)^\mu + \frac{g_S}{2\Lambda}(k+p)^\mu + \frac{g_{T^+}}{2\Lambda}\iota\sigma^{\mu\nu}(k+p)_\nu \quad (1)$$

$$\Gamma_A^\mu = g_A\gamma^\mu\gamma_5 + \frac{f_E}{2\Lambda}\iota\sigma^{\mu\nu}(k-p)_\nu\gamma_5 + \frac{g_{P^-}}{2\Lambda}(k-p)^\mu\gamma_5 + \frac{g_P}{2\Lambda}(k+p)^\mu\gamma_5 + \frac{g_{T_5^+}}{2\Lambda}\iota\sigma^{\mu\nu}(k+p)_\nu\gamma_5\,. \quad (2)$$

In this paper, in consideration of the additional Lorentz structures to pure $V-A$, we consider the g_i or Λ_i as complex phenomenological parameters. For $g_L = 1$ units with $g_i = 1$, the nominal size of Λ_i is $\frac{m_t}{2} = 88GeV$, see [1]. In the SM, the EW energy-scale is set from the Higgs-field vacuum-expectation-value by the parameter $v = \sqrt{-\mu^2/|\lambda|} = \sqrt{2}\langle 0|\phi|0\rangle \sim 246GeV$.

The helicity formalism is based on the assumption of Lorentz invariance but not on any specific discrete symmetry property of the fundamental amplitudes, or couplings. For instance, for $t \to W^+b$ and $\bar{t} \to W^-\bar{b}$ a specific discrete symmetry implies a definite symmetry relation among the associated helicity amplitudes. In the case of $\tilde{T}_{FS}$ invariance, the respective helicity amplitudes must be purely real,

$$A^*(\lambda_{W^+}, \lambda_b) = A(\lambda_{W^+}, \lambda_b) \quad (3)$$

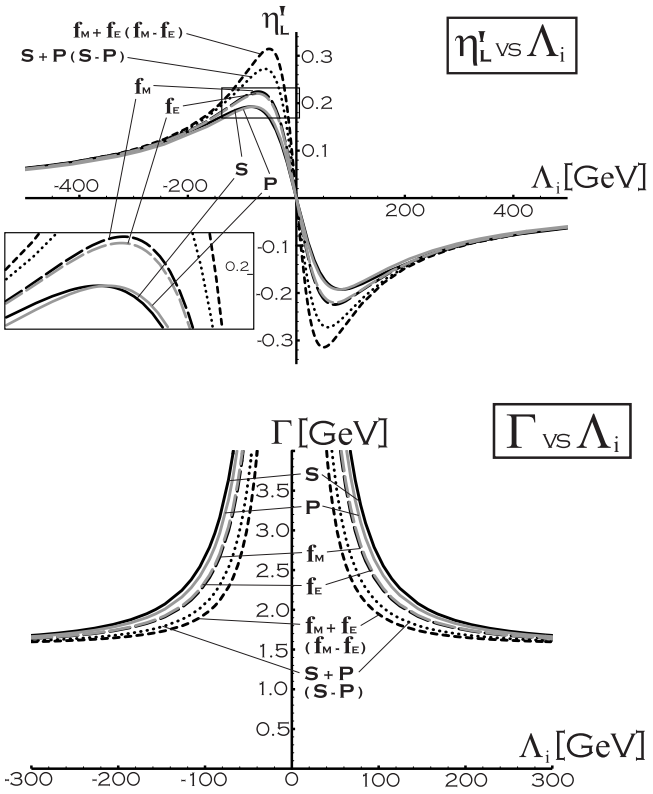

Fig. 1. The first *five sets of figures* are for the case of a single additional pure-imaginary coupling, $ig_i/2\Lambda_i$ or ig_i, associated with a specific additional Lorentz structure, $i = S, P, S+P, \ldots$. The two plots displayed here are for dimensional couplings with chiral $S \pm P$, $f_M \pm f_E$ and non-chiral S, P, f_M, f_E Lorentz structures. The *upper plot* displays the $\eta_L{}'$ helicity parameter versus the effective-mass scale Λ_i with $g_i = 1$ in $g_L = 1$ units. The *lower plot* displays the induced effect of the additional coupling on the partial width for $t \to W^+b$. The standard model(SM) limit is at the "wings" where $|\Lambda_i| \to \infty$

$$B^*\left(\lambda_{W^-}, \lambda_{\bar{b}}\right) = B\left(\lambda_{W^-}, \lambda_{\bar{b}}\right). \tag{4}$$

Intrinsic and relative signs of the helicity amplitudes are specified in accordance with the standard Jacob-Wick phase convention. $\tilde{T}_{FS}$ invariance will be violated if either (i) there is a fundamental violation of canonical "time reversal" invariance, or (ii) there are absorptive final-state interactions. In the SM, there are no such final-state interactions at the level of sensitivities considered in the present analysis. To keep this assumption of "the absence of final-state interactions" manifest, we refer to this as $\tilde{T}_{FS}$ invariance, see [15] and references therein. If experimental evidence for $\tilde{T}_{FS}$ violation were found, it would be very important to establish whether (i), (ii), or some combination of the two effects was occurring. For instance, unexpected final-state interactions might be associated with addition t-quark decay modes.

To assess future measurements of helicity parameters in regard to $\tilde{T}_{FS}$ violation, Figs. 1–5, are for the case of a single additional pure-imaginary coupling, $ig_i/2\Lambda_i$ or ig_i, associated with a specific additional Lorentz structure, $i = S, P, S+P, \ldots$. In the SM, all the relative phases are either zero or $\pm\pi$ so all of the primed helicity parameters are zero.

2.1 Additional $S \pm P$, , $f_M \pm f_E$, S, P, f_M, or f_E couplings

The two plots displayed in Fig. 1 are for dimensional couplings with chiral $S \pm P$, $f_M \pm f_E$ and non-chiral S, P, f_M, f_E Lorentz structures. The upper plot displays the $\eta_L{}'$ helicity parameter versus the effective-mass scale Λ_i with $g_i = 1$ in $g_L = 1$ units. This parameter is defined by

$$\eta_L' \equiv \frac{1}{\Gamma}\left|A\left(-1, -\frac{1}{2}\right)\right|\left|A\left(0, -\frac{1}{2}\right)\right|\sin\beta_L \tag{5}$$

where $\beta_L = \phi_{-1}^L - \phi_0^L$ is the relative phase difference the two helicity amplitudes in (5). The peaks of the curves shown in the upper plot do not however correspond to where $|\sin\beta_L| \sim 1$. Instead, at the peaks $|\sin\beta_L| \sim 0.6 - 0.8$. The lower plot displays the induced effect of the additional coupling on the partial width for $t \to W^+b$. The SM model limit is at the "wings" where $|\Lambda_i| \to \infty$ for each additional dimensional coupling. If the R-handed b-quark amplitudes were found not to be negligible, it would be important to consider both $\eta_{L,R}'$ or equivalently both η' and ω'.

Figure 2 displays plots of the b-polarimetry interference parameters $\epsilon_+{}'$ and $\kappa_0{}'$ versus Λ_i for the case of a single additional S, P, f_M, f_E and $S \pm P, f_M - f_E$ coupling. These helicity parameters are defined by

$$\begin{aligned}\kappa_0' &\equiv \frac{1}{\Gamma}\left|A\left(0, \frac{1}{2}\right)\right|\left|A\left(0, -\frac{1}{2}\right)\right|\sin\alpha_0 \\ \epsilon_+' &\equiv \frac{1}{\Gamma}\left|A\left(1, \frac{1}{2}\right)\right|\left|A\left(0, -\frac{1}{2}\right)\right|\sin\gamma_+\end{aligned} \tag{6}$$

where $\alpha_0 = \phi_0^R - \phi_0^L$ and $\gamma_+ = \phi_1^R - \phi_0^L$ are the relative phases between the two amplitudes in (6). In the SM, the analogous κ_0, ϵ_+ in which the cosine function replaces the sine function are the two $\mathcal{O}(LR)$ helicity parameters involving the L-handed amplitude with the largest modulus. Unfortunately, the tree-level values of κ_0, ϵ_+ in the SM are only about 1%. Two dimensional plots of the type (ϵ_+, η_L) and (κ_0, η_L), and of their primed counterparts, have the useful property that the unitarity limit is a circle of radius 0.5 centered on the origin.

In both plots, the peaks in the curves do correspond respectively to where $|\sin\alpha_0| \sim 1$ and $|\sin\gamma_+| \sim 1$, except those for S, P in the lower $\kappa_0{}'$ plot where $|\sin\alpha_0| \sim 0.8$ at the peaks. The drops in the curves for small $|\Lambda_i|$'s is due to the vanishing of the sine of the corresponding relative phase. Curves are omitted in the plots in this paper when the couplings produce approximately zero deviations in the helicity parameter of interest, e.g. this occurs for $f_M + f_E$ in both the $\epsilon_+{}'$ and $\kappa_0{}'$ helicity parameters.

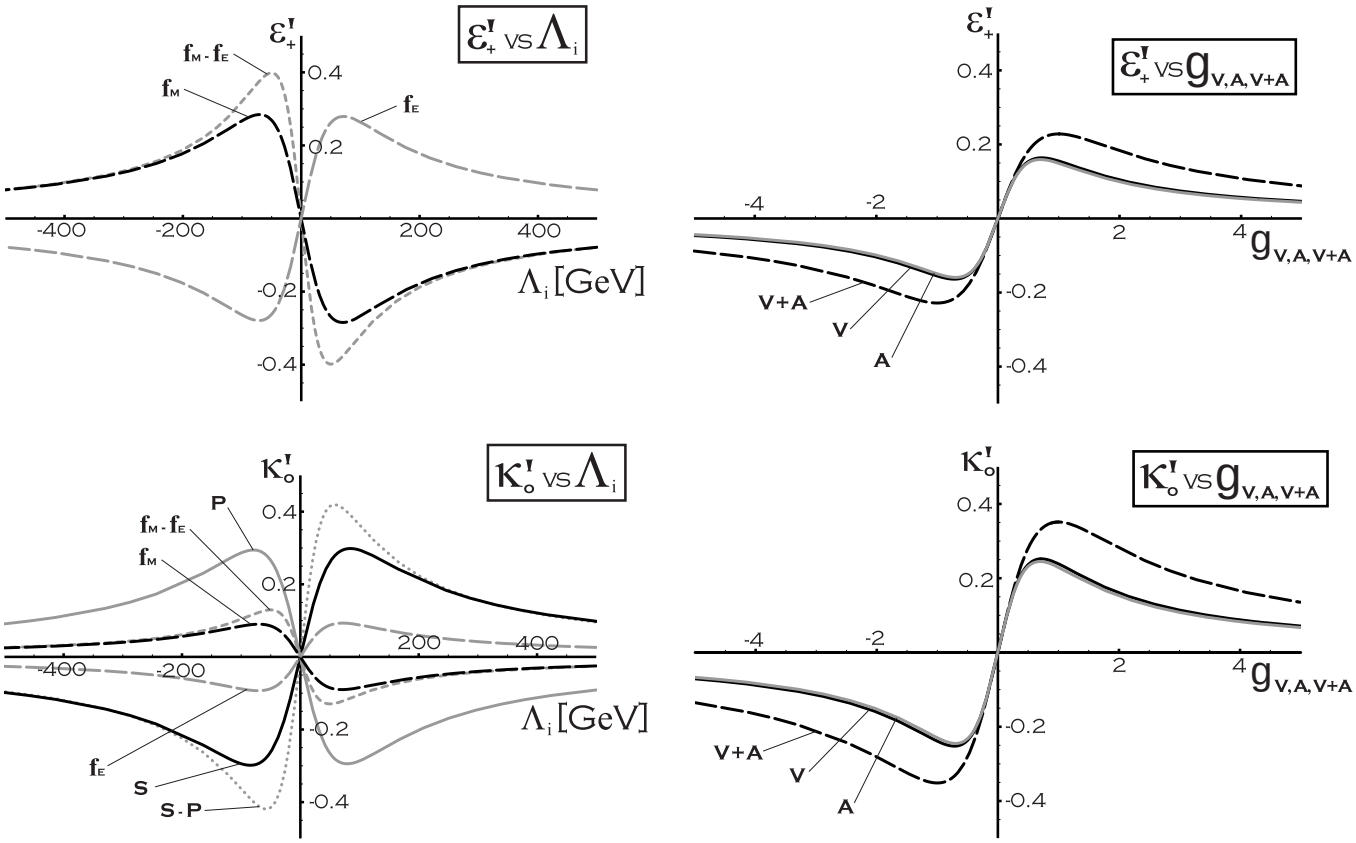

Fig. 2. Plots of the b-polarimetry interference parameters $\epsilon_+{}'$ and $\kappa_0{}'$ versus Λ_i for the case of a single additional S, P, f_M, f_E and $S \pm P, f_M - f_E$ coupling. Curves are omitted in the plots in this paper when the couplings produce approximately zero deviations in the helicity parameter of interest

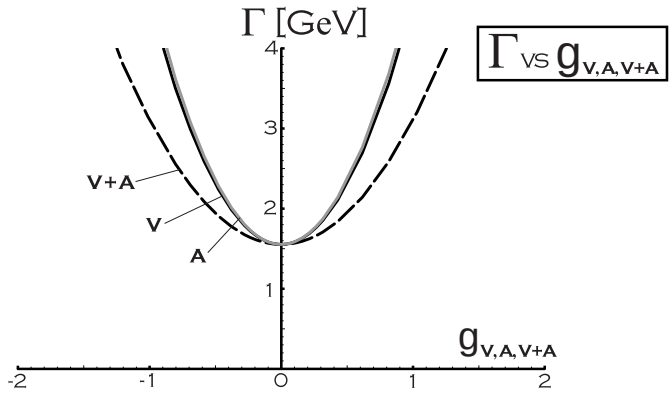

Fig. 3. For a single additional gauge-type coupling V, A, or $V + A$, plots of the b-polarimetry interference parameters $\epsilon_+{}'$ and $\kappa_0{}'$, and of the partial width for $t \to W^+b$ versus pure-imaginary coupling constant ig_i. There is not a significant signature in η'_L due to the $\tilde{T}_F S$ violation "masking mechanism" associated with gauge-type couplings [15]. The g_i value is in $g_L = 1$ units. The SM model limit is at the origin, $g_i \to 0$

2.2 Additional $V + A$, V, or A couplings

An additional $V - A$ type coupling with a complex phase versus the SM's g_L is equivalent to an additional overall complex factor in the SM's helicity amplitudes. This will effect the overall partial width Γ, but it doesn't effect the other helicity parameters.

For a single additional gauge-type coupling V, A, or $V + A$, in Fig. 3 are plots of the b-polarimetry interference parameters $\epsilon_+{}'$ and $\kappa_0{}'$, and of the partial width for $t \to W^+b$ versus pure-imaginary coupling constant ig_i. The g_i value is in $g_L = 1$ units. In the cases of the additional dimensionless, gauge-type couplings, the SM model limit is at the origin, $g_i \to 0$. The peaks for the $V + A$ coupling do correspond to where the associated sine of the relative phase has maximum magnitude; instead, for the V, A couplings, $|\sin\alpha_0| \sim 0.8$ $|\sin\gamma_+| \sim 0.8$ at the peaks.

2.3 Indirect effects of $\tilde{T}_{FS}$ violation on other helicity parameters

The plots in Fig. 4 show the indirect effects of a single additional pure-imaginary chiral coupling, $ig_i/2\Lambda_i$ or ig_i, on other helicity parameters. For the coupling strength ranges listed in the "middle table", the upper plot shows the effects on the probability, $P(W_L)$, that the emitted W^+ is "Longitudinally" polarized and the effects on the probability, $P(b_L)$, that the emitted b-quark has "Left-handed" helicity. Each curve is parametrized by the magnitude of the associated g_i or Λ_i. On each curve, the central open circle corresponds to the region with a max-

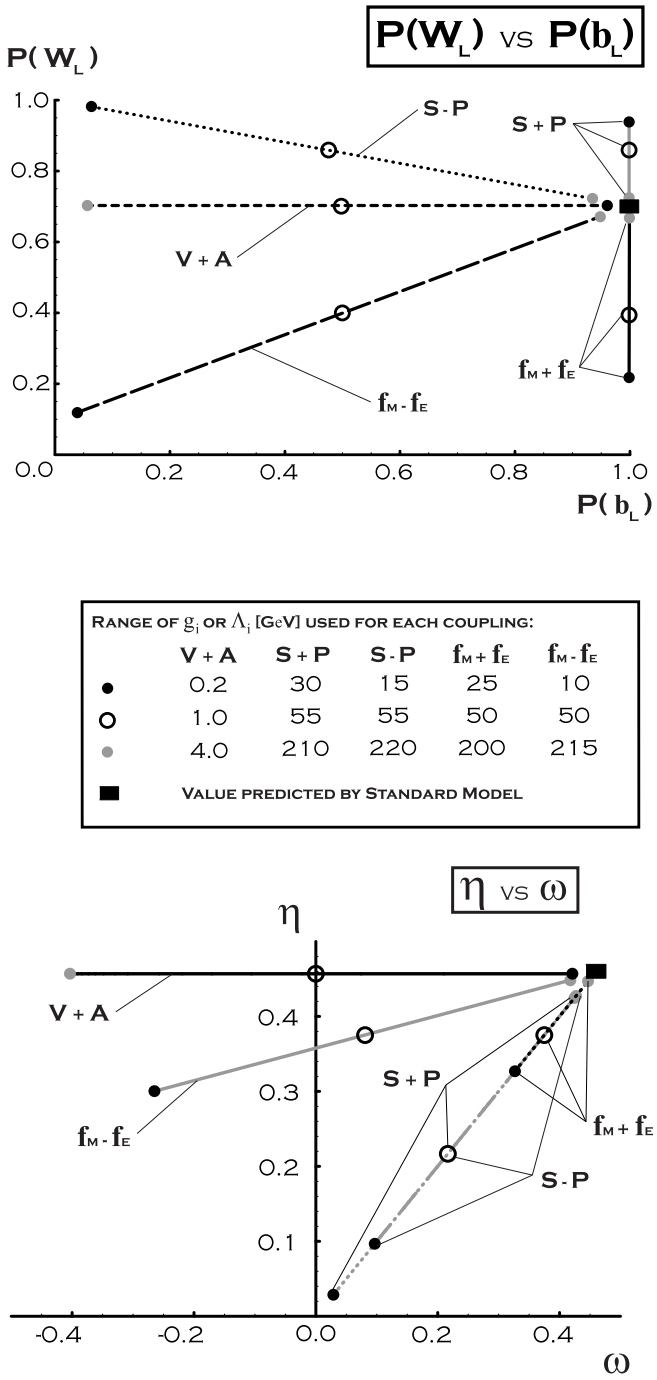

Fig. 4. These plots show the indirect effects of a single additional pure-imaginary chiral coupling, $ig_i/2\Lambda_i$ or ig_i, on other helicity parameters. A dark rectangle denotes the value for the SM. For the coupling strength ranges listed in the "middle table", the *upper plot* shows the indirect effects on the probabilities $P(W_L)$ and $P(b_L)$. Each curve is parametrized by the magnitude of the associated g_i or Λ_i. On each curve, the central open circle corresponds to the region with a maximum direct $\tilde{T}_{FS}$ violation signature. The dark/light solid circles correspond respectively to the ends of the ranges listed in the middle table where the direct signatures fall to about 50% of their maximum values. The *lower plot* is for the W-polarimetry interference parameters η, ω

imum direct $\tilde{T}_{FS}$ violation signature, e.g. for $f_M + f_E$ from Fig. 1 this is at $|\Lambda_{f_M+f_E}| \sim 50GeV$. The dark/light solid circles correspond respectively to the ends of the ranges listed in the middle table where the direct signatures fall to about 50% of their maximum values. Similarly the lower plot is for the W-polarimetry interference parameters η, ω. Curves are omitted for the remaining moduli parameter ζ, the pre-SSB parameter which characterizes the odd-odd mixture of the b and W^+ polarizations [15], because a single additional pure-imaginary coupling in these ranges produces approximately zero deviations from the pure $V - A$ value of $\zeta = 0.41$.

The plots in Fig. 5 show the indirect effects of a single additional pure-imaginary non-chiral coupling on other helicity parameters. Versus the middle table given here, the curves are labeled as in Fig. 4.

It is instructive to compare the above plots with their analogues in [1]. Unlike in the analogous plots in [1], finite m_b effects do not lead to sizable "oval shapes" in plots in this paper because interference terms must vanish in intensities arising from the sum of a real $V - A$ amplitude and the pure-imaginary $ig_i/2\Lambda_i$ or ig_i amplitude.

In summary, sizable $\tilde{T}_{FS}$ violation signatures can occur for low-effective mass scales ($< 320GeV$) as a consequence of pure-imaginary couplings associated with a specific additional Lorentz structure. However, in most cases, such additional couplings can be more simply excluded by 10% precision measurement of the probabilities $P(W_L)$ and $P(b_L)$. In most cases, the W-polarimetry interference parameters η and ω can also be used as indirect tests, or to exclude such additional couplings.

3 Tests for $\tilde{T}_{FS}$ violation associated with the dynamical phase-type ambiguities

The purpose of this section is to consider the situation when the $\tilde{T}_{FS}$ violation exists in the decay helicity amplitudes, but nevertheless does not significantly show up in the values of the moduli parameters. We call this 'partially hidden $\tilde{T}_F S$ violation."

Based on the notion of a complex effective mass scale parameter $\Lambda_X = |\Lambda_X| \exp(-i\theta)$ where θ varies with the mass scale $|\Lambda_X|$, we exploit the dynamical phase-type ambiguities to construct two simple phenomenological models in which this happens. When $\sin\theta \geq 0$, the imaginary part of Λ_X could be interpreted as crudely describing a more detailed/realistic dynamics with a mean lifetime scale $\Gamma_X \sim 2|\Lambda_X| \sin\theta$ of pair-produced particles at a production threshold $Re[2\Lambda_X]$. For $\sin\theta \leq 0$, fundamental time-reversal violation or a new dynamics might approximately correspond to such a complex Λ_X. In the case of the $f_M + f_E$ ambiguity, over the full θ range, this construction does preserve the magnitudes' puzzle, see Sect. 1, between the $V - A$ and $f_M + f_E$ lines in the lower part of Table 1.

$S + P$ dynamical, phase-type ambiguity: In Fig. 6 are plots of the signatures for a partially-hidden $\tilde{T}_{FS}$ vio-

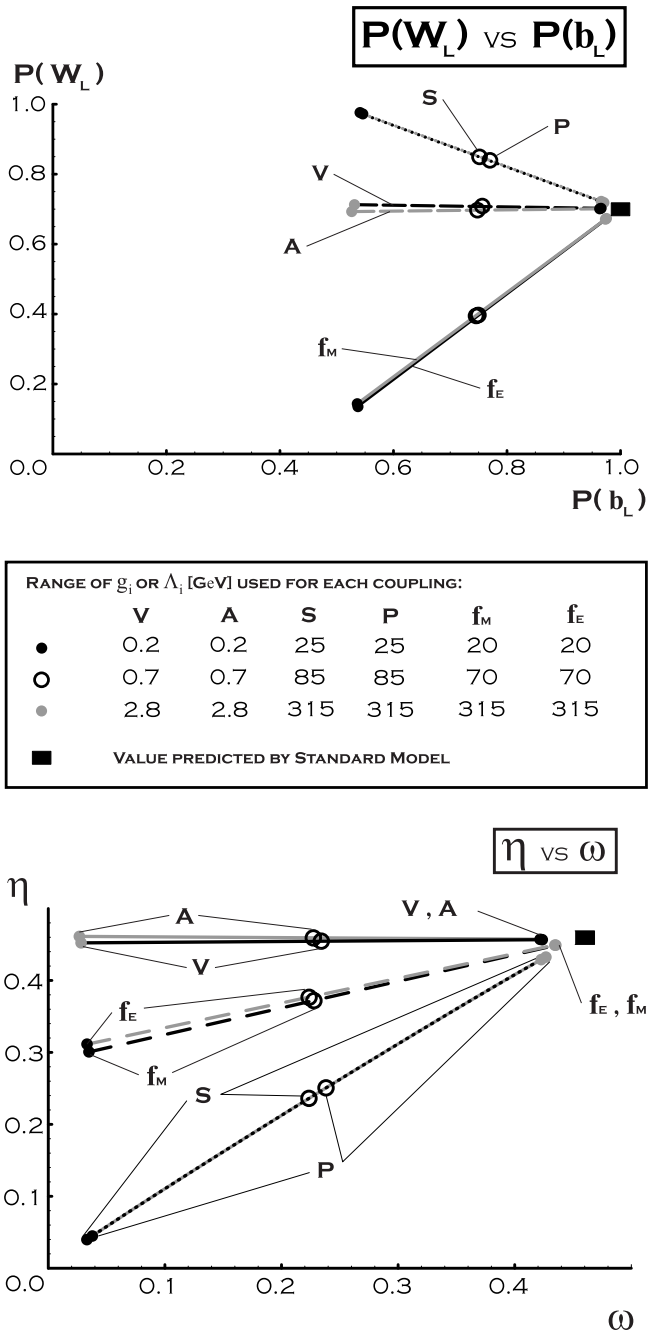

Fig. 5. These plots show the indirect effects of a single additional pure-imaginary non-chiral coupling on other helicity parameters. Versus the middle table given here, the curves are labeled as in Fig. 4. The *upper plot* is for the two probabilities $P(W_L)$ and $P(b_L)$. The *lower plot* is for η, ω

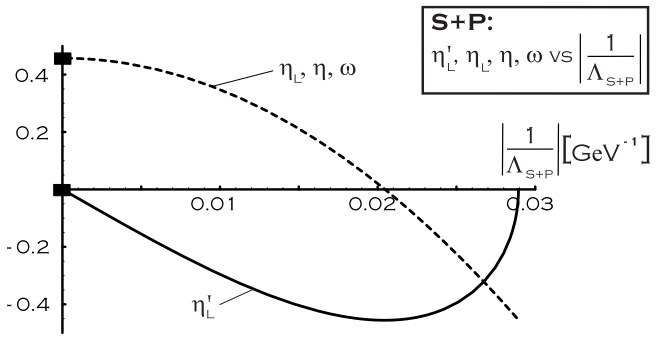

Fig. 6. Plots of the signatures for a partially-hidden $\tilde{T}_{FS}$ violation (see text) associated with a $S+P$ phase-type ambiguity. Plotted versus $1/|\Lambda_{S+P}|$ for the case $\sin\theta \geq 0$ is the solid curve for $\eta_L{}'$, and the dashed curve for η_L, η, ω which are degenerate

lation associated with a $S+P$ phase-type ambiguity. We require $|A_X(0,-\frac{1}{2})| = |A_L(0,-\frac{1}{2})|$ to hold when the additional $S+P$ coupling, $g_{S+P}/2\Lambda_{S+P}$ has a complex effective mass scale parameter $\Lambda_{S+P} = |\Lambda_{S+P}|\exp(-i\theta)$ where θ varies with the mass scale $|\Lambda_{S+P}|$. For $m_b = 0$, the resulting relationship is $\cos\theta \simeq -\frac{m_t}{4\Lambda}(1-(\frac{m_W}{m_t})^2)$ for $34.5GeV \leq |\Lambda_{S+P}| \leq \infty$ which correspond respectively to $\pm\pi \geq \theta \geq \pm\frac{\pi}{2}$. This construction maintains the standard model values in the massless b-quark limit for the four moduli parameters, $P(W_L), P(b_L), \zeta$, and Γ. The function $\theta(|\Lambda_{S+P}|)$ is then used for the $S+P$ coupling when $m_b = 4.5GeV$. The SM values for the moduli parameters are essentially unchanged. The phase choice of $\phi^R{}_1 = \pm\pi$, cf. top line in Table 1, has no consequence since it is a 2π phase difference.

For $\sin\theta \geq 0$, in Fig. 6 the solid curve shows $\eta_L{}'$ plotted versus $1/|\Lambda_{S+P}|$. The dashed curve is for η_L, η, ω which are degenerate. The dark rectangles show the standard model values at the $|\Lambda_{S+P}| \to \infty$ endpoint. At the other endpoint $|\Lambda_{S+P}| \sim 34.5GeV$, or $1/|\Lambda_{S+P}| = 0.029GeV^{-1}$.

From the perspectives of (i) measuring the W interference parameters and of (ii) excluding this type of $\tilde{T}_{FS}$ violation, it is noteworthy that where $\eta_L{}'$ has the maximum deviation, there is a zero in η_L, η, ω. So if the latter parameters were found to be smaller than expected or with the opposite sign than expected, this would be consistent with this type of $\tilde{T}_{FS}$ violation.

At the maximum of $\eta_L{}'$, $|\Lambda_{S+P}| \sim 49GeV$ and the other $\tilde{T}_{FS}$ violation parameters are also maximum. The curves for these parameters have the same over all shape as $\eta_L{}'$ but their maxima are small, $\epsilon_+{}' \sim 0.015$ and $\kappa_0{}' \sim 0.028$. For the other case where $\sin\theta \leq 0$, all these $\tilde{T}_{FS}$ violation primed parameters have the opposite overall sign. The signs of other helicity parameters are not changed.

$f_M + f_E$ dynamical, phase-type ambiguity: In Fig. 7 are plots of the signatures for a partially-hidden $\tilde{T}_{FS}$ violation associated with a $f_M + f_E$ phase-type ambiguity. As above for the analogous $S+P$ construction, the additional $f_M + f_E$ coupling $g_{f_M+f_E}/2\Lambda_{f_M+f_E}$ now has an effective mass scale parameter $\Lambda_{f_M+f_E} = |\Lambda_{f_M+f_E}|\exp(-i\theta)$ in which θ varies with the mass scale $|\Lambda_{f_M+f_E}|$ to maintain standard model values in the massless b-quark limit for the moduli parameters $P(W_L), P(b_L)$, and ζ. For $X = f_M + f_E$, we require $\frac{|A_X(-1,-\frac{1}{2})|}{|A_X(0,-\frac{1}{2})|} = \frac{|A_L(-1,-\frac{1}{2})|}{|A_L(0,-\frac{1}{2})|}$ so for $m_b = 0$ the relationship giving $\theta(|\Lambda_{f_M+f_E}|)$ is $\cos\theta \simeq \frac{m_t}{4\Lambda}(1+(\frac{m_W}{m_t})^2)$ for $52.9GeV \leq |\Lambda_{f_M+f_E}| \leq \infty$ which corre-

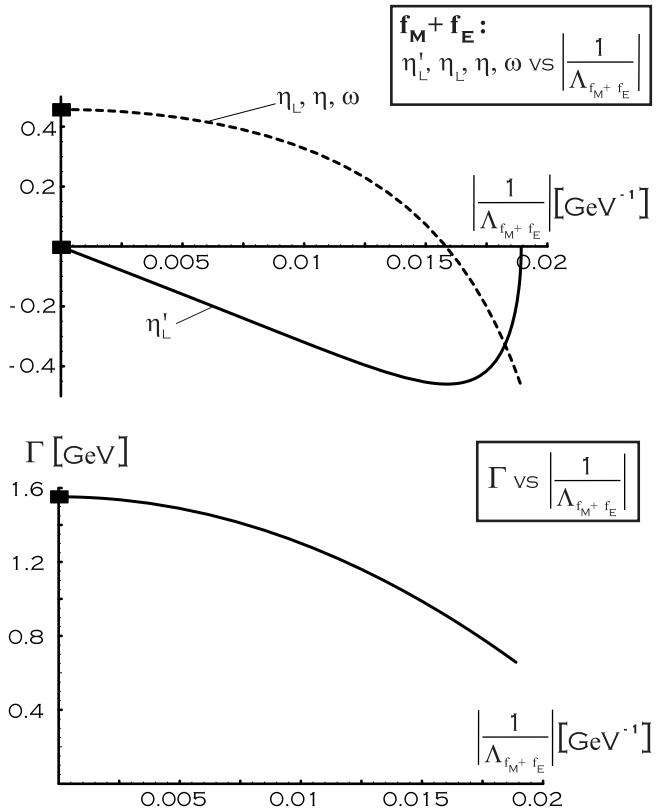

Fig. 7. Plots of the signatures for a partially-hidden $\tilde{T}_{FS}$ violation (see text) associated with a $f_M + f_E$ phase-type ambiguity. Versus $1/|\Lambda_{f_M+f_E}|$ for $\sin\theta \geq 0$, the *upper plot* shows by the solid curve $\eta_L{}'$, and by the dashed curve η_L, η, ω. The *lower plot* shows the indirect effect of such a coupling on the partial width

spond respectively to $0 \leq \theta \leq \pm\frac{\pi}{2}$. For the case $\sin\theta \geq 0$, in Fig. 7 the upper plot shows by the solid curve $\eta_L{}'$ versus $1/|\Lambda_{f_M+f_E}|$. By the dashed curve, it shows η_L, η, ω. At the endpoint $|\Lambda_{f_M+f_E}| \sim 52.9GeV$, or $1/|\Lambda_{f_M+f_E}| = 0.0189GeV^{-1}$.

Here, as in Fig. 6, where $\eta_L{}'$ has the maximum deviation, there is a zero in η_L, η, ω. The lower plot shows the indirect effect of such a coupling on the partial width Γ. While $|\Lambda_{f_M+f_E}|$ varies, two of the relative phases remain almost fixed, $\gamma_\pm \sim \pm\pi$ respectively, so only one independent relative phase could be viewed as driving the variation, e.g. β_L varies from $-\pi$ to zero.

At the maximum of $\eta_L{}'$, $|\Lambda_{f_M+f_E}| \sim 63GeV$. The curve for $\kappa_0{}'$ has the same shape and is also maxmimum at the same position with a value $\kappa_0{}' \sim 0.005$. There is a zero in κ_0 at this position. $\epsilon_+{}'$ remains very small and $\epsilon_+ \simeq -0.015$. For the other case, $\sin\theta \leq 0$, each of these $\tilde{T}_{FS}$ violation primed parameters has the opposite overall sign. Since $\text{sign}(-\sin\phi_0^L) = \text{sign}(\sin\phi_0^R) = \text{sign}(\sin\theta)$ and $\text{sign}(-\sin\phi_{-1}^L) = \text{sign}(\sin\phi_1^R) = \text{sign}(\sin\theta)$, all the relative phases change sign for the case $\sin\theta \leq 0$.

In summary, sufficiently precise measurement of the W-interference parameters η_L and $\eta_L{}'$ can exclude such partially-hidden $\tilde{T}_{FS}$ violation associated with either of the two dynamical phase-type ambiguities. However, if $\eta_L = (\eta + \omega)/2$ were found to be smaller than expected or with a negative sign, such a measurement would be consistent with this type of $\tilde{T}_{FS}$ violation.

Acknowledgements. For computer assistance, one of us (CAN) thanks John Hagan and Ted Brewster. This work was partially supported by U.S. Dept. of Energy Contract No. DE-FG 02-86ER40291.

References

1. C.A. Nelson and A.M. Cohen, Eur. Phys. J. **C8**, 393 (1999). In the case of the $S+P$ ambiguity, Table 2 should list $\kappa_0 = 0.05$, i.e. with a positive sign. See also C.A. Nelson and L.J. Adler, hep-ph/0006342, contributed paper for ICHEP2000
2. The CDF collaboration reported that the fraction of longitudinal W bosons is $F_0 = 0.91 \pm 0.37 \pm 0.13$ assuming a pure $V-A$ coupling, T. Affolder, et.al., Phys.Rev.Lett. **84**, 216 (2000); the DØ collaboration reported $t\bar{t}$ spin-correlation results in B. Abbott, et.al., Phys.Rev.Lett. **85**, 256 (2000)
3. M.Beneke, et. al., hep-ph/0003033, to appear in "1999 CERN Workshop on SM physics (and more) at the LHC"
4. D. Atwood, S. Bar-Shalom, G. Eilam, and A. Soni, hep-ph/0006032
5. Reports from a top quark workshop at Fermilab include G. Mahlon hep-ph/9811219, hep-ph/9811281; S.S. Willenbrock, hep-ph/9905498
6. W. Bernreuther, A. Brandenburg, and Z.G. Si, Phys.Lett. **B483**, 99 (2000); W. Bernreuther, A. Brandenburg, and M. Flesch, hep-ph/9812387
7. M. Fischer, S. Groote, J.G. Körner, M.C. Mauser, B. Lampe, Phys.Lett. **B451**, 406 (1999); B. Lampe, hep-ph/9801346
8. B. Grzadkowski, Z. Hioki, Phys.Rev. **D61**, 014013 (2000); hep-ph/0003294
9. G. Mahlon and S. Parke, Phys.Lett. **B476**, 323 (2000); hep-ph/0001201; J. Kodaira, T. Nasuno, S. Parke, hep-ph/9807209
10. T. Tait, Phys. Rev. **D61**, 0340001 (2000); F. Larios and C.-P. Yuan, Phys.Lett. **B457**, 334 (1999); T. Tait and C.-P. Yuan, hep-ph/9710372
11. Y. Kiyo, J. Kodaira, K. Morii, T. Nasuno, and S. Parke, hep-ph/0006021
12. J. Guasch, W. Hollik, J. I. Illana, C. Schappacher, and J. Sola, hep-ph/0003109; C. Macesanu and L.H. Orr, hep-ph/0001138
13. E. Boos, M. Dubinin, M. Sachwitz, and H.J. Schreiber, hep-ph/0001048; A.Belyaev and E. Boos, hep-ph/0003260; A.Belyaev, hep-ph/0007058
14. M. Jack, A. Hoefer, A. Leike, and T. Riemann, hep-ph/0007046
15. C.A. Nelson, B.T. Kress, M. Lopes, and T.P. McCauley, Phys. Rev. **D56**, 5928 (1997); **D57**, 5923 (1998)